*Desalination and Water Treatment*
www.deswater.com

doi: 10.5004/dwt.2019.23889

154 (2019) 72–81
June

# Modeling and experimental study of air gap membrane distillation unit: application for seawater desalination

Imen El Mokhtar[a,*], Ali Boubakri[a], Salah Al Tahar Bouguecha[b], Amor Hafiane[a]

[a]*Laboratory of Water, Membranes and Environmental Biotechnology, Center of Researches and Water Technologies, P.B 273, 8020 Soliman, Tunisia, Tel. +216 52 533 545; email: elmokhtarimen@gmail.com*
[b]*Department of Mechanical Engineering, Faculty of Engineer, King Abdul-Aziz University, P.B: 80204 Jeddah 21589, Saudi Arabia*

Received 4 January 2018; Accepted 28 January 2019

**ABSTRACT**

The single stage air gap membrane distillation (AGMD) has been successfully realized to desalt simulated and natural seawater. The effect of different operating parameters including feed temperature, width of air gap, feed salt concentration and feed and permeate flow rates on the performance of AGMD process has been investigated. Two different commercial polyvinylidene fluoride (PVDF) membranes, with different pore size (0.45 and 0.22 μm) were tested and compared for different operating parameters. Experimental results displayed that the larger pore size membrane showed a better mass transfer performance but led to a slight decrease of water production quality. However, AGMD process can produce water with high salt rejection, more than 99% and a maximum permeate flux of 9.06 kg $m^{-2}$ $h^{-1}$ was obtained at a feed temperature of 77°C. The comparison between predicted model and experimental AGMD permeate fluxes shown a good agreement, their average deviation was around 6.9%.

*Keywords:* AGMD; Desalination, PVDF membrane; Mass transfer; Seawater

## 1. Introduction

Recently, Fresh water shortage is an important problem for many countries. The economically and technologically viable solution to tackle this challenge is the water desalination that offers a seemingly unlimited supply of high-quality of pure water [1]. Desalination technologies mainly divided on thermal and membrane separation processes. Nevertheless, each one of the above methods presents some drawbacks. Thermal process has lost favor due to its high-energy demand, then it presents a lower specific power consumption and, consequently, relatively lower specific water production cost [2]. Reverse osmosis (RO) currently dominated the desalination of seawater application. However, the drawbacks of this process are associated to height operating pressure, environmental impact of the rejected brine and fouling phenomena [3].

As an emerging method for water treatment and desalination, membrane distillation (MD) is a new hybrid process, which combines phase-change thermal distillation and membrane separation technologies [4]. MD is a thermally driven process that uses a hydrophobic membrane as a contactor separating the two dissimilar temperature fluids. The trans-membrane vapor pressure difference created by the vapor/liquid equilibrium at the micro-porous membrane serves as the driving force. In this separation technology, the membrane often acts as a physical barrier between hot and cold fluids, hence, it has no effects on the process selectivity [5]. Interest in MD quickly rose in the early 80s due to the development of new polymers that provided membranes with adequate characteristic for the application [6]. Increasingly, MD is taken into consideration and is being considered as a viable alternative substitute to other prominent desalination process due to their unique technical advantages where the greatest one lies in its requirement

* Corresponding author.

of low grade energy associated with its ability to operate at lower hydrostatic pressure that make it more attractive than conventional pressure-driven membrane separation processes such as RO. Furthermore, it is a low temperature water removal process unlike the conventional distillation process which makes it better suited for use with low temperature heat sources then it is able to use renewable energies such as solar and geothermal energy. Additionally, it has a great potential on the application for low-grade wastewater resource utilization, due to the increasing of global warming, that made it more promising separation process [7–9].

Based on the condensation permeate ways, there are different methods to maintain the trans-membrane vapor pressure difference to drive the flux, such as [4]: (1) direct contact membrane distillation (DCMD); in which the hydrophobic membrane is in direct contact with feed fluids and the cold one is on the other face to remove distillate. (2) Sweeping gas membrane distillation (SGMD); it is a complicated system design, therefore, it is the least used configuration, an external condenser is sweep to collect permeate water, where a stripping gas is used for this purpose. (3) Vacuum membrane distillation (VMD); is the most promising MD configurations where the permeate side is a light air under reduced pressure created using a vacuum pumps. (4) Air gap membrane distillation (AGMD); this configuration is one of the famous and the most studied varieties of the MD process. It has the capability to draw attention because of its compact installation unlike in SGMD and VMD systems those in need of external condensers [10]. In the AGMD systems, a stagnant air layer separates the membrane from a cold condensing wall located parallel to the membrane which collects vapor diffused by the pressure difference across the gap to the permeate side inside the membrane module [1].

Compared with other MD methods, AGMD has favorable heat transfer with highest thermal efficiency because of the introduction of air gap in the membrane module which have insulation and resistance properties. This reduces significantly the direct thermal loss by conduction and temperature polarization. Besides, because of this interval gap, the contamination of distillate by the feed solution has less chance to happen, hence collection of distillate becomes easier, then low chance to surface membrane wetting [4]. Moreover, in contrast to VMD, in the air gap MD system, the vapor is condensed at the local saturation temperature. Hence, the creative design of AGMD and its thermal proprieties make this configuration competitive with more founded base-thermal technologies and in major part, the product from the evaporation/condensation process in the AGMD unit is not only fresh water when it is applied in desalination technology but also it can be extensively employed for most industrial applications, mainly where energy accessibility is low. Also, it has the possibility to separate some volatile substance such as alcohols [11] and nitric acid [12] from aqueous solution which cannot be removed in DCMD system [13] and isotopic water separation [14].

Previous studies have widely validated that AGMD could be effectively applied for desalination of seawater. Recently researches on AGMD focused on the parameters that have an effect on their performances. However, until now, researches about modeling desalination using AGMD process have been considered only in very few studies. Geng et al. [15] used a new air-gap membrane distillation module for salt removal from synthetic water using parallel hollow fiber membranes. It was obtained a maximum permeate flux of 5.30 kg $m^{-2}$ $h^{-1}$. Another study was conducted by Xu et al. [16] which assumes the performance of two membranes with various pore sizes on AGMD systems using synthetic NaCl solutions. They stated that when the pore size increases, the permeate flux increases. They interpreted the influences of feed inlet temperature and water circulation rate on water flux and distillate quality. However, they did not apply their results on seawater desalination. Dehesa-Carrasco et al. [17] studied the influences of various parameters on air gap membrane distillation process, it has been found that the feed temperature has an important effect on the increase of the permeate flux, for instance, increasing the feed temperature from 40°C to 70°C causes about 590% rise in the permeate flux and in laminar regime. Alkhudhiri et al. [18] investigated the influence of operating parameters on AGMD performances. It was found that the permeate flux is directly proportional to the feed temperature and the feed flow rate. However, it is inversely proportional to the feed concentration and coolant temperature. The impact of air-gap width was reported by Asghari et al. [19], who found that the permeate flux increases by 3.5-fold when reduced air-gap width from 25 to 5 mm.

The aim of this study was to investigate the feasibility and the performance of AGMD process using polyvinylidene fluoride (PVDF) membranes with different pore size (0.22 and 0.45 μm) to desalt both synthetic solution and real seawater. The effects of operating parameters on permeate flux and rejection factor were carried out including feed temperature, air gap width, initial salt concentration, and flow rates and validate the predicted permeate fluxes by the experiments results.

## 2. Model development

### 2.1. Membrane domain

In AGMD process, the permeate flux ($J_p$) is proportional to the vapor pressure difference across the membrane matrix. For laminar flow, the permeate flux can be expressed by Darcy's law according to the following equation [20]:

$$J_p = B_m \left( P_{\mathrm{mf}} - P_{\mathrm{mp}} \right) \tag{1}$$

$$J_p = \frac{K_m}{\sqrt{M}} \left( P_{\mathrm{mf}} - P_{\mathrm{mp}} \right) \tag{2}$$

where $B_m$ is the membrane coefficient, it is dependent on membrane characteristic and feed temperature, $M$ is the molecular weight of water, and $P_{\mathrm{mf}}$ and $P_{\mathrm{mp}}$ are the vapor pressures at the feed, and permeate vapor/liquid interfaces, respectively, and permeate vapor/liquid interfaces, respectively, and are related to the activity of the solution by the following equation [21]:

$$P_{\mathrm{mi}} = \xi_i \times P^0_{\mathrm{im}} \qquad i = f, i \tag{3}$$

where $\xi_i$ is the water activity and $P^0_{\mathrm{im}}$ is the pure water vapor pressure and can be evaluated using Antoine equation [22]:

$$P_{\text{im}}^{0} = \exp\left(A - \frac{B}{C+T}\right) \tag{4}$$

$T$ in Kelvin, $P_{\text{im}}^{0}$ in Pascal, $A$, $B$ and $C$ are constants which can be determined by the regression of experimental measures, for AGMD: $A$ = 23.273, $B$ = 3,841.2 and $C$ = –45.

The vapor pressure composition can be estimated as Eq. (5), according to Raoult's law [23].

$$P_{\text{mi}} = \left(1 - x_{\text{mi}}\right) P_{\text{mi}}^{0} \tag{5}$$

where $x_{\text{mi}}$ is the mole fraction of the solute at the membrane interface.

Mathematically, for a binary or a ternaries unideal solution, the liquid/vapor equilibrium describes the partial pressure ($P_{\text{mi}}$) according to this thermodynamic relation: $P_{\text{mi}} = P_{\text{im}}^{0}\, x_i\, \xi_i$.

In MD process, according to the dusty-gas model, three mechanisms control the diffusive mass transfer across the pores of hydrophobic membrane, including Knudsen diffusion, molecular mechanism and combined (Knudsen-molecular) [1].

#### 2.1.1. Knudsen diffusion

The relative equations dominating the mass transfer mechanism based on membrane coefficient. The mass transfer coefficient or the permeability coefficient in a gas mixture with a uniform pressure throughout the system [24].

$$B_m^{k} = \frac{\varepsilon \times dp}{\left(3\chi \times \delta\right) \times \sqrt{\frac{8Me}{\pi RT}}} \tag{6}$$

where ε, $d_p$, and δ are the porosity of the membrane, pore diameter and the membrane thickness, respectively, $R$ is the gas constant, $T$ is the absolute temperature, χ is the membrane tortuosity and it is determined using Eq. (7):

$$\chi = \frac{2-\varepsilon}{\varepsilon} \tag{7}$$

#### 2.1.2. Molecular diffusion

The transport of the vapor through the membrane can be modeled by the molecular diffusion mechanism when the pore size of the membrane is much bigger than the molecular mean free path of water vapor [13]. In this mechanism, the mass transfer coefficient can be calculated from the following expression:

$$B_m^{D} = \frac{\varepsilon \times PD \times Me}{\chi \times \delta \times Pa \times RT} \tag{8}$$

PD (Pa m$^2$ s$^{-1}$) is the air diffusion coefficient determined using Eq. (9) [13,23].

$$\text{PD} = 1.895 \times 10^{-5} \times T^{2.072} \tag{9}$$

$P_a$ is the air pressure, and $D$ is the water diffusion:

$$P_{\text{air}} = P - P_{\text{mf}} \tag{10}$$

#### 2.1.3. Combined diffusion

The mass transport takes place via a combined Knudsen/ordinary diffusion mechanism. In AGMD configuration, the following model was used to determine the permeability through the membrane pores and can be calculated using the following expression:

$$B_m^{C} = \left[\frac{3\delta\pi}{\varepsilon d_p}\sqrt{\frac{\pi RT}{8M_w}} + \frac{\chi\delta P_a RT}{\varepsilon \text{PD}_w M_w}\right]^{-1} \tag{11}$$

To judge the dominating mechanism of the mass transfer in the pores, the Knudsen number is used [25]:

$$Kn = \frac{\lambda}{dp} \tag{12}$$

The mean free path can be calculated by using the following expression [23]:

$$\lambda = \frac{K_B \times T_m}{\pi\left(\frac{\sigma_w - \sigma_a}{2}\right)^2 \times P \times \sqrt{1 + \left(\frac{M_w}{M_a}\right)}} \tag{13}$$

where $K_B$ is the Boltzmann constant (1.381 × 10$^{-23}$ J K$^{-1}$), $P$ is the total pressure inside the pore, $T_m$ is the average membrane temperature, ($\sigma_w$ = 2.641 × 10$^{-10}$ m) and $\sigma_a$ (3.711 × 10$^{-10}$ m) is the collision diameters for water vapor and air, respectively, $M_w$ and $M_a$ are the molecular weights of water and air, respectively [26].

### 2.2. Air gap domain

The air gap is interposed inside the membrane module to reduce the direct thermal loss by conduction and temperature polarization. In AGMD, for the steady state, the expression diffusion of water vapor through a stagnant air film can be written as follows [19].

$$J_v = \frac{M_v c D}{\delta_g}\left(\frac{P_{\text{mg}}}{P} - \frac{P_{\text{gf}}}{P}\right) \tag{14}$$

where $c$ is the total molar concentration, $\delta_g$ is the air gap width, $P_{\text{gf}}$ is the partial vapor pressure in the interface air gap/condensation film, $P_{\text{mg}}$ is the partial vapor pressure in the interface air gap/membrane.

## 3. Materials and methods

### 3.1. AGMD setup

The experimental setup of AGMD is schematically shown in Fig. 1,the experimental set up was functioned in

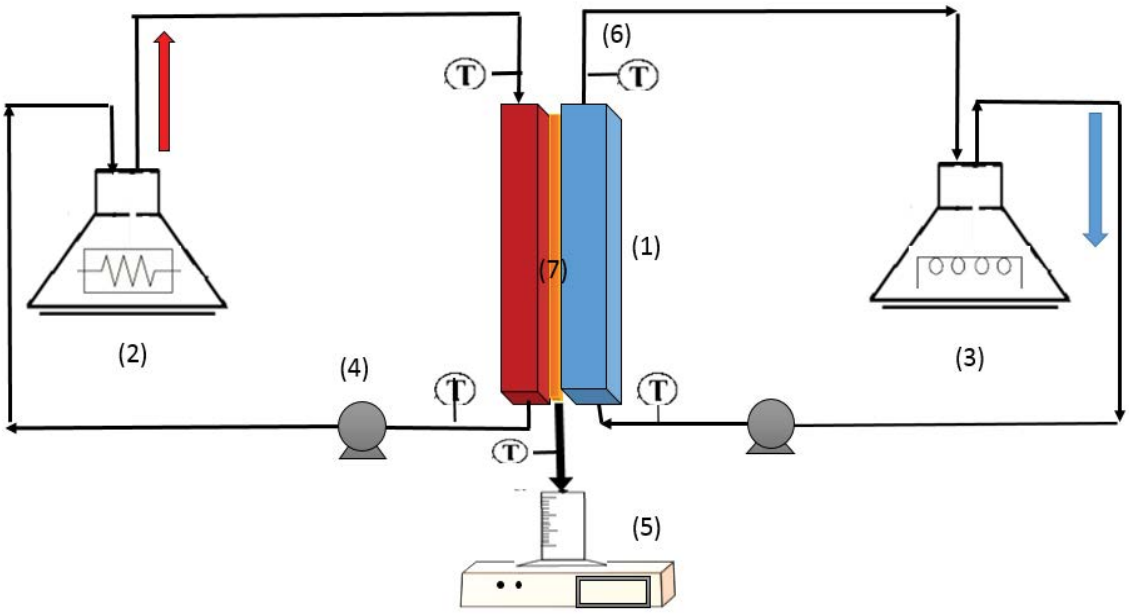


Fig. 1. Schematic diagram of AGMD setup: (1) flat sheet module, (2) feed tank, (3) cooling element, (4) peristaltic pumps, (5) permeate water, (6) thermocouples and (7) membrane.

counter-current flow configuration using flat sheet PVDF membrane (0.45 and 0.22 μm pore size) made by Millipore. This membrane was held between two Plexiglass chambers; at one side of the unit, a saline solution, which is connected to a heating system, is maintained in direct contact with the hydrophobic membrane while the other one was closed by an aluminum coolant plate (0.5 mm) where introduced an air gap. The air gap thickness was varied (3, 5, 7 and 9 mm) of acrylic frames inserted between the membrane and condensation plate. The permeate vapor diffused through the membrane and condensed on the aluminum foil. Phase change occurs at this hydrophobic membrane interface, according to the vapor–liquid equilibrium. The effective membrane area placed between the two compartments is 0.0032 $m^2$. The temperatures of the feed and cold solution at five points (two inlets and three outlets) were measured with digital thermometer with an accuracy of ±0.1°C. The feed and permeate solution were pumped using two peristaltic pumps with adjustable flow rate. The permeate electric-conductivity monitoring was performed by means of conductivity meter.

### 3.2. PVDF membrane

Two commercially flat sheet hydrophobic microporous membranes made with PVDF polymer with different pores size are used in our AGMD pilot scale. Table 1 presents the principal characteristics of used membranes as specified by manufacturers and completed by others analysis techniques.

The membrane characterization was performed using the following methods:

The liquid entry pressure (LEP) measurement can determine the minimum hydrostatic pressure must be applied to a feed water to penetrate into dry membrane pore. LEP value was measured agreeing with the method reported by Boubakri et al. [27]. It is shown in Table 1 that the LEP values of both membranes PVDF 0.22 and 0.45 μm were about 207 and 186 kPa, respectively. The two values were higher than water vapor pressure at the studied temperature between 50°C and 90°C. Those values can be explained by the relationship between pore size and LEP; high LEP may be reached using a membrane material with a small pore size.

Table 1
Characteristics of PVDF membrane

| Material | PVDF 1 | PVDF 2 |
|---|---|---|
| Nominal pore size | 0.22 μm | 0.45 μm |
| Thickness | 125 μm | 125 μm |
| Porosity | 75% | 75% |
| Manufacturer | Millipore, GVHP | Millipore, HVHP |
| Contact angle | 109.15° | 101.6° |
| Liquid entry pressure | 207 ± 2 kPa | 186 ± 2 kPa |
| Effective membrane area | $3.2 \times 10^{-3}$ m | $3.2 \times 10^{-3}$ m |

The optical tension-meter (Attension Theta) with automated liquid pumping system is a guide of hydrophobicity of the tow membrane via the measurement of the membrane contact angle (CA). The CA measurement (Fig. 2) for virgin membranes surfaces by calculating the average of four different points of the membrane sample. The values of CA for two PVDF membranes illustrated by Figs. $2a_1$ and $a_2$, respectively, were 109.75° for PVDF 0.22 μm membrane and 101.62° for PVDF 0.45 μm membrane, which gives information on the excellent hydrophobic character of two kinds of membrane. Therefore, high hydrophobicity may be achieved using a membrane material with a small pore size.

The scanning electron microscope (FEI Quanta FEG 250 SEM) was used to characterize the PVDF membrane

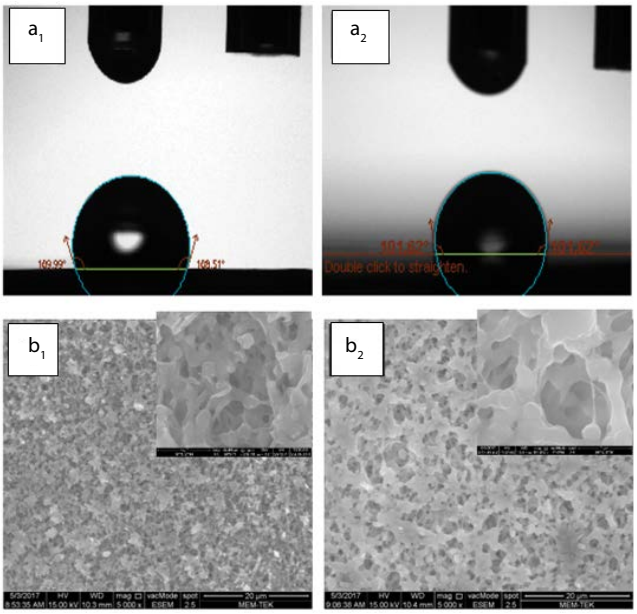


Fig. 2. (($a_1$) and ($a_2$)) Contact angle and (($b_1$) and ($b_2$)) SEM membrane characterization.

morphologies. Fig. 2 shows the SEM images of surface of virgin membranes (0.22 and 0.45 μm pore size) with magnification 20 μm. The difference between the two membranes is clearly visible. Morphology of the investigated membranes PVDF (0.22 μm) collated in Fig. $2b_1$ are more compact, dense and homogeneous in structure. Whereas the morphology of PVDF (0.45 μm) membrane presented in Fig. $2b_2$ displays a homogeneous porous structure, which possess more open structure and a degree of porosity around 75%.

### 3.3. Performance indicators for AGMD process

The principle performance indicators of AGMD process are the permeate flux $J_p$ and the quality of the permeate water measured by the electric conductivity using a conductivity/pH meter (Consort C561). $J_p$ (kg m$^{-2}$ h$^{-1}$) was calculated by the following equation:

$$J_p = \frac{\Delta m}{A \times \Delta t} \tag{15}$$

where $\Delta m$ is the weight of permeate (kg), $A$ is the effective membrane area (m$^2$) and $\Delta t$ is the sampling time (h).

The salt removal efficiency could be defined according to the flowing equation:

$$r = \left(1 - \frac{C_p}{C_0}\right) \times 100 \tag{16}$$

where $C_p$ is permeate salt concentration and $C_0$ (mg L$^{-1}$) is the initial feed salt concentration (mg L$^{-1}$).

### 3.4. Experimental procedure

The AGMD experiments consist of analyzing the feasibility and the performance of the system under different operating parameters. Synthetic salt solution, and seawater were used as feed solutions. Different NaCl concentrations (5–30 g L$^{-1}$) were prepared as a feed solution by dissolving a reagent grade NaCl salt (supplied by Honeywell Fluka) in distilled water. The feed water operating conditions included different inlet temperatures (50°C–90°C) and inlet flow rates varied (3 to 36 L h$^{-1}$). The operating conditions of the cooling water were flow rates: 3–36 L h$^{-1}$. The seawater was obtained from the Mediterranean coast of Tazerka, northern of Tunisia and was used without any pre-treatment step. The physico-chemical characteristics of the raw water are summarized in Table 2.

## 4. Results and discussion

### 4.1. Validation of model results

Mass transfer has been investigated in the range 50°C–90°C. Three different transfer models, as previously cited, were employed to describe the mass transfer across the membrane matrix. The behavior of different predicted models was compared with the experimental data as function of inlet feed temperature to determine the suitable mass transfer mechanism through the PVDF 0.22 μm membrane used in AGMD process. Fig. 3 shows that the permeate fluxes increase exponentially by increasing feed temperature, which is in agreement with other AGMD studies [2]. This can be explained by the exponential increase of the vapor pressure with temperature according to the Antoine equation which leads to an exponential enhance in the driving force, increasing the temperature gradient across the membrane and the air gap will positively affect the diffusion coefficient. Furthermore, the viscosity of feed solution is reduced when increasing temperature, therefore the mass transfer was increased.

The comparison between experimental and calculated permeate flux showed that the combined Knudsen-molecular model is the dominant diffusive mass transfer model for AGMD using PVDF membrane. The maximum and minimum error percentages between the theoretical and experimental models are 6.99% and 4.27%, respectively.

To confirm the agreement between the predicted and experimental models, the Knudsen number ($K_n$) was

Table 2
Physico-chemical composition of seawater

| Parameter | Value |
|---|---|
| Temperature (°C) | 25 |
| Conductivity (mS cm$^{-1}$) | 26.7 |
| pH | 7.51 |
| $Cl^-$ | 21.27 |
| $SO_4^{2-}$ | 2.91 |
| $HCO_3^-$ | 0.162 |
| $K^+$ (g L$^{-1}$) | 0.55 |
| $Ca^{2+}$ (g L$^{-1}$) | 0.35 |
| $Na^+$ (g L$^{-1}$) | 17 |
| $Mg^{2+}$ (g L$^{-1}$) | 0.993 |
| TDS (g L$^{-1}$) | 43.6 |

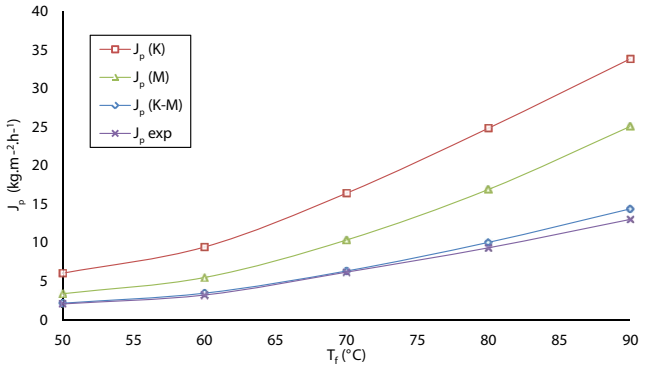


Fig. 3. Modeled and experimental permeate fluxes vs. feed temperature ($T_p$ = 23°C; $Q_f = Q_c$ = 20 L h$^{-1}$; $\delta_g$ = 3 mm).

calculated from Eqs. (12) and (13). For this study, the pore size of the two PVDF membrane used are 0.22 and 0.45 μm. Then, for both cases, $K_n$ calculated was in the range of 0.463 and 0.49 for PVDF membrane (0.22 μm) and in the range of 0.225 and 0.24 for PVDF membrane (0.45 μm). As $0.01 < K_n < 1$, the combined Knudsen-molecular model is correspondingly confirmed to be the appropriate transfer mechanism across the PVDF membrane for AGMD.

For all experimental runs using PVDF membrane, the maximum measured value of electrical conductivity is below 20.3 μS cm$^{-1}$, with a rejection factor of NaCl more than 98.7%.

### 4.2. Effect of flow rate

The combined effect of feed and coolant flow rates on AGMD permeate flux using two different commercial PVDF membranes with various pore size (0.22 and 0.45 μm) is shown in Fig. 4. The feed flow rate varied from 6 to 36 L h$^{-1}$ at constant feed temperature of 70°C, coolant temperature of 23°C and air gap width of 3 mm. For both different PVDF membranes, increasing the feed flow rate causes a rise of permeate flux from about 2.5-folds.

The effect of hydrodynamic conditions on mass transfer is strongly dependent on Reynolds number. Increasing the flow rate leads to changing the circulation from Re < 300 (corresponding to flow rate of 1.5 L min$^{-1}$) to Re > 300 that in turn enhances driving force for mass transfer through the membrane, and thus decreases the influence of both temperature and concentration polarization phenomenon. This causes increasing the AGMD permeate flux.

For higher feed flow rates, the permeation flux reaching an asymptotic value due to the reduction in the boundary layer's thickness when the Re approaching a limiting value [28]. Consequently, it can be a good compromise working with a flow with low level of turbulence. The permeate flux is plotted as a function of $Q_f$ and $Q_c$ in Fig. 5. It can be observed that increasing both factors results in an enhancement of AGMD flux, but the effect of coolant flow rate was less significant than the effect of feed flow rate on permeate flux on production rate. It is evident that when increasing the feed and coolant flow rate, the water production rate varies in a different manner. Nevertheless, the feed flow rate was sensibly controlled to keep the membrane safe from

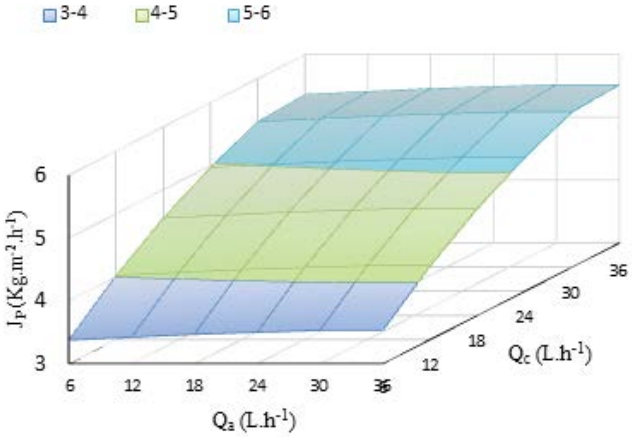


Fig. 5. Surface plot of permeate flux as function of feed flow rate and coolant flow rate.

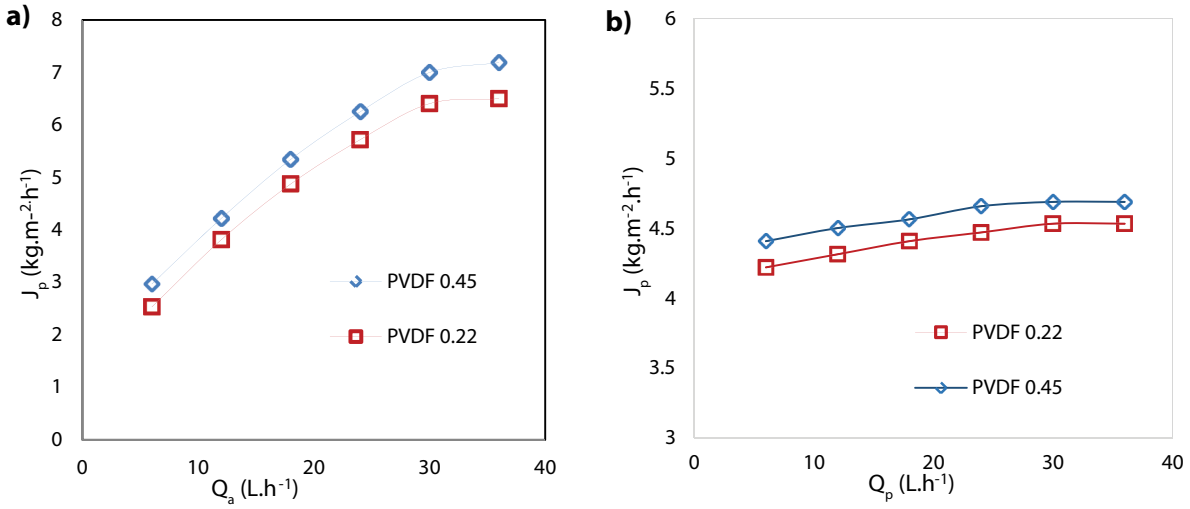


Fig. 4. Variation in flux with (a) increased feed flow and (b) increased coolant flow.

mechanical destruction as very high flow rate would press the membrane against the support and therefore would cause distorted membrane pores [29].

It can be noted that a salt rejection rate higher than 99.60% was found for all the experiments with different pore size of PVDF membrane, and was not influenced by the feed and coolant flow rates.

### 4.3. Effect of feed salinity

The influence of feed salt concentration on permeate flux for two kinds of membranes (0.22 and 0.45 um) has been studied in the range of 5–30 g $L^{-1}$ for feed and coolant inlet temperatures of 70°C and 23°C, respectively. Fig. 5 displays the variation of permeate flux as function of feed salt concentration. It was observed that the increase of feed sodium chloride concentration leads to a slight decrease of permeate flux. The permeate production reduced only by 3.6% for PVDF membrane (0.45 μm) and by 5.7% for PVDF membrane (0.22 μm). This trend can be attributed to the fact that dissolved NaCl in the feed solution decreases slightly the partial vapor pressure and consequently reduces the driving force which leads to reduced performance of the AGMD process in term of permeate production [15,30]. Moreover, the concentration polarization increases with salt concentration, which in turn decreases the mass transfer coefficient of the boundary layer.

On the other hand, the rejection factor shows linear behavior with small decline in the studied range of feed salt concentration, but kept more than 98.8% at high concentration of 30 g $L^{-1}$. The slight decrease of the permeate quality can be attributed to the membrane wettability phenomenon. In this case, the vapor diffusion will be associated with the phenomenon of salt swiping.

### 4.4. Effect of air gap width

AGMD process is considered to be the most energy efficient compared with other MD configurations because the transport resistances in the air/vapor gap normally dominate the thermal performance causing a degradation in permeate production [9]. The performance of AGMD process using PVDF membrane as a function of air gap width in the range 3–9 mm is presented in Fig. 6. At a constant inlet feed salt concentration of 45 g $L^{-1}$, feed temperature of 70°C and $T_c$ of flow rate of 20 L $h^{-1}$, the results show that permeate flux reduced significantly from 5.84 to 3.59 kg $m^{-2}$ $h^{-1}$ (1.62-fold) for PVDF (0.45 μm) membrane and from 5.28 to 2.9 kg $m^{-2}$ $h^{-1}$ (1.82-fold) for PVDF (0.2 μm) membrane with increasing air gap width from 3 to 9 mm. In the light of this result, it is expected that the mass transfer was controlled by diffusion for $\delta_g$ < 5 mm while convection started to take place for $\delta_g$ > 5 mm and a linear trend of the distillate flux is observed [31]. The effect of air gap thickness on permeate flux is almost significant over the range taken in this study since it gives an extra mass transfer resistance which is commonly found in the AGMD process. This result can be explained by the fact that the presence of air gap is efficient to avoid heat conduction loss because of the low thermal conductivity of the air relative to other domain between hot and cold solution. Consequently, the shorter the gap width, the shorter is the diffusion path and the lower is the mass transfer resistance and thus, the AGMD production is higher [24,32].

The permeate conductivity as a function of increasing air gap thickness is shown in Fig. 7. An increase of $\delta_g$ in the studied range can lead to a slight increasing permeate conductivity from 5.9 to 12.7 μS $cm^{-1}$. AGMD process can produce a high-quality fresh water improved after desalting solution with high salinity.

### 4.5. Application of AGMD for seawater

Seawater without any pretreatments was desalted by AGMD process using PVDF membrane with different pore size (0.22 and 0.45 μm). The physico-chemical compositions of this water are presented in Table 2. The AGMD operating conditions were transmembrane temperature difference of 47°C, feed and coolant flow rates of 20 L $h^{-1}$ and air gap width of 3 mm. The experimental results of the permeate flux and conductivity during 45 h are presented in Fig. 8. It can be observed, for both membranes, that the permeate flux reduces slightly as function of time. For membrane with 0.22 μm pore size, the permeate flux decreases from 3.81 to 3 kg $m^{-2}$ $h^{-1}$. The result showed dual significant decline in the permeate

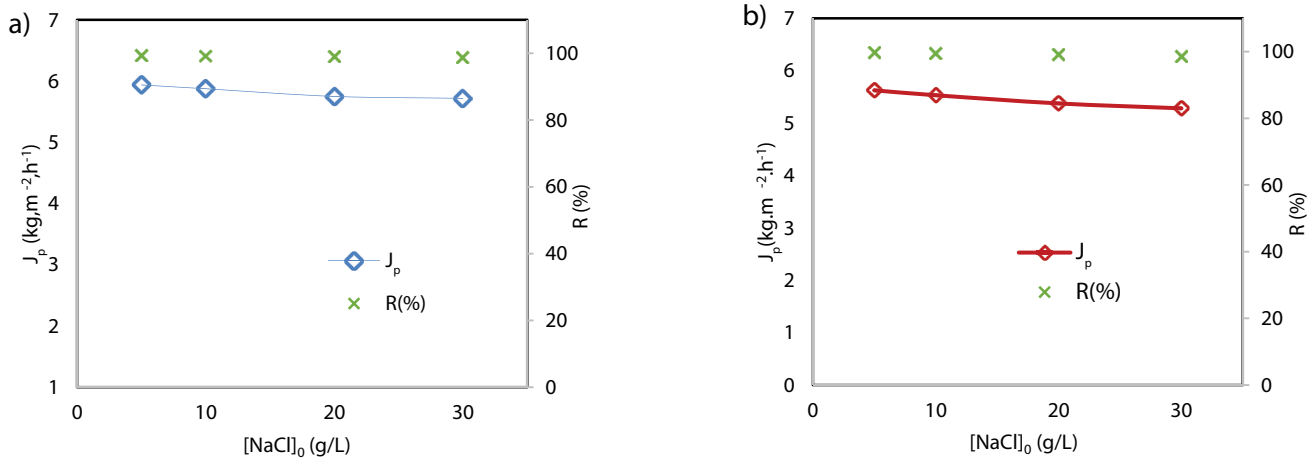


Fig. 6. Effect of initial NaCl concentration on AGMD permeate flux using (a) PVDF membrane 0.45 μm and (b) PVDF membrane 0.22 μm.

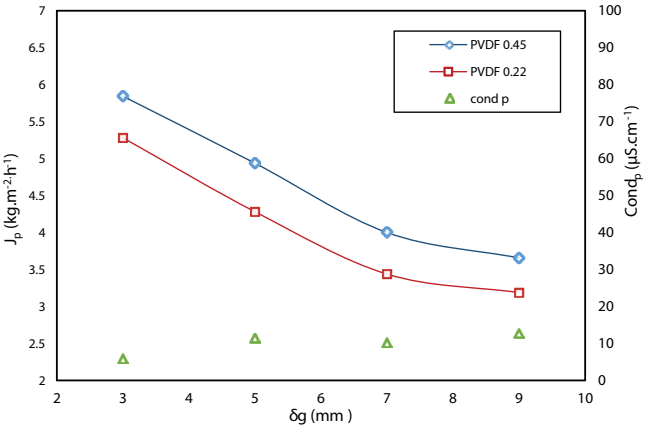


Fig. 7. Effect of air gap thickness on permeate flux.

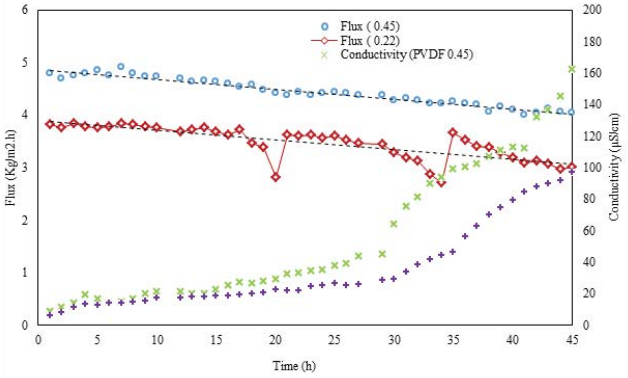


Fig. 8. Performance of AGMD during long-term operation for seawater.

flux every 18 h of running that was corrected by simple water washing of the membrane surface that can be explained by the reduction of the surface CA measurement. For PVDF (0.45 µm) membrane, the permeate flux decreases from 4.78 to 4.03 kg m$^{-2}$ h$^{-1}$. It is evident that the operation period is found to be quite stable during the experiments lasting for 45 h, this is in agreement with the previously obtained results carried out on the effect of initial salt concentration which has a slight effect on permeate flux. It can be seen that water flux increased by 21.7% with increasing pore size. The reason is that the mass transfer within the pores was enhanced with increasing pore size, which is dominated by the Knudsen diffusion mechanism that results in a better vapor permeability and consequently, the AGMD production is higher.

For a long running period, the obtained results of desalination of seawater, without pretreatment, the electrical conductivity of permeate relatively was below the recommended values for drinking water. The permeate conductivity increased for both types of membrane as a function of time. In the case of membrane with larger pore size, the permeate conductivity increases from 8.9 to 162 µS cm$^{-1}$ after 45 h of operation. This can be attributed to the membrane wettability and diminished the hydrophobicity of membrane due to the presence of high amount of organic matter and total dissolved substances in seawater which can be transported through the wetted pores to the distillate side. On the other hand,

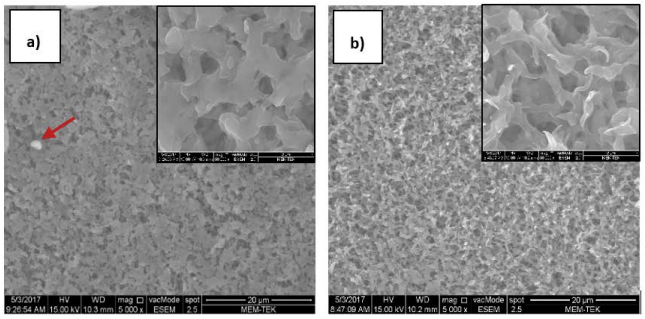


Fig. 9. SEM images taken for the (a) PVDF (0.22 µm) and (b) PVDF (0.45 µm).

the results of long period AGMD application of seawater without any pretreatment showed that the PVDF (0.22 µm) membrane had slightly decreased permeate flux during 45 h. The permeate conductivity had slightly increased, reached 97.2 µS cm$^{-1}$ due to partial membrane pores wettability. Nevertheless, it can be observed that PVDF (0.22 µm) presented an excellent salt rejection (higher than 99.9%) on the other hand PVDF with pore size of 0.45 µm showed less salt rejection, only 99.4%. Generally, the larger pore size showed a better mass performance but led to decrease in the quality of distillate due to the higher conductivity values. In light of this result, an optimum value of pore size is needed to be determined for each MD application depending on the type of the feed solution to be salted [31].

Figs. 9a and b presents the SEM observations taken for the membrane surface using PVDF (0.22 µm) and PVDF (0.45 µm), respectively. SEM micrograph observations illustrate the difference between morphology for virgin membrane surface and for PVDF membrane after long AGMD operating for seawater. The microstructure of the two PVDF membranes was not significantly affected by the long running AGMD operation for seawater. However, the micrograph of two membrane shows a slight accumulation of suspended solids at the membrane surface and pores after 45 h of operation which causes the membrane scaling and then the decrease of permeate flow of the process and increase the electrical conductivity of permeate water.

These experimental results confirm that desalination of seawater by AGMD process using PVDF membrane (0.22 and 0.45 µm) can produce a high water quality with low electrical conductivity under the recommended values for drinking water.

## 5. Conclusion

AGMD process using PVDF membrane with different pore size is a feasible promising alternative process to desalt saline solutions and seawater. The effect of relevant operating parameters including feed temperature, feed and coolant flow, initial salt concentration and the design parameter of the module such as width of air gap were studied.

The experimental permeate flux presents a good agreement with the mass transfer, based on the combined Knudsen-molecular diffusion model can be explained by the simplifying supposition of one-directional flow through feed chamber of the module. The feed temperature is the

most important parameter in AGMD permeate flux. The performance of this system increases exponentially as the feed inlet temperatures rise. At 73°C, PVDF (0.45 μm) membrane showed the higher permeate flux of 6.11 kg $m^{-2}$ $h^{-1}$ than the PVDF (0.22 μm) membrane with a permeate flux of 5.34 kg $m^{-2}$ $h^{-1}$. The AGMD permeate flux was also affected by hydrodynamic conditions. Hence, increasing both factors marks a sensitive enhancement of AGMD flux, but the effect of feed flow rate is more significant than coolant flow rate. Air gap width have a significant negative effect on permeate flux. At 73°C, using PVDF (0.45 μm) membrane, the results show that permeate flux showed that permeate flux reduced significantly from 5.28 to 2.9 kg $m^{-2}$ $h^{-1}$ and from 5.84 to 3.59 kg $m^{-2}$ $h^{-1}$ for PVDF (0.2 μm) membrane with increasing air gap width from 3 to 9 mm. The parametric study results showed that, for an AGMD process, the initial NaCl concentration has not been capable of drawing much attention with a slightly decreasing permeate flow. PVDF (0.22 μm) and PVDF (0.45 μm) membranes reached a very high salt rejection above 99.80% for all experimental runs, and under the same operating conditions, PVDF membrane with highest pore size showed the greater permeate flux but the lower salt rejection.

The results of long-period AGMD application of seawater without any pretreatment had a slightly decreasing permeate flux for both PVDF membranes during 45 h. The permeate conductivity had slightly increased, reached 97.2 μS $cm^{-1}$ after 45 h for desalting seawater using PVDF (0.22 μm) and a sharp increase was obtained to reach 162 μS $cm^{-1}$ for desalting seawater using PVDF (0.45 μm) due to partial membrane pores wettability.

## Symbols

$a_w$ — Water activity
$B_m$ — Membrane distillation coefficient, kg $m^{-2}$ $s^{-1}$ $Pa^{-1}$
$K_m$ — Permeability coefficient
$d_p$ — Pore diameter, m
$D_w$ — Diffusion coefficient for water, $m^{-2}$ $s^{-1}$
PD — Air diffusion coefficient, Pa $m^{-2}$ $s^{-1}$
$J_p$ — Permeate flux, kg $m^{-2}$ $h^{-1}$
$k_B$ — Boltzmann constant, $1.380 \times 10^{-23}$ J $K^{-1}$
$K_n$ — Knudsen number
$M$ — Molecular weight, kg $kmol^{-1}$
Nu — Nusselt number
$P$ — Total pressure inside the pore, Pa
$P_{mf}$ — Vapor pressure at the feed side of the membrane surface, Pa
$P_{mp}$ — Vapor pressure at the permeate side of the membrane surface, Pa
Pr — Prandtl number
$R$ — Gas constant, J $mol^{-1}$ $K^{-1}$
$R$(%) — Rejection rate, %
$C_p$ — Permeate salt concentration, mg $L^{-1}$
$C_0$ — Feed salt concentration, mg $L^{-1}$
Re — Reynolds number
$T$ — Temperature, K
$x_{mi}$ — Mole fraction of solute at the membrane interface

## Greek

Δ — Membrane thickness, m
ε — Membrane porosity
χ — Membrane tortuosity
λ — Mean free path, m
σ — Collision diameter, m
ρ — Density of water, kg $m^{-3}$
ν — Linear velocity of water, m $s^{-1}$
μ — Dynamic viscosity of water, kg $m^{-1}$ $s^{-1}$

## Subscripts

*f* — Feed
*p* — Permeate
*m* — Membrane
*a* — Air
*w* — Water

## References

[1] H. Geng, Q. He, H. Wu, P. Li, C. Zhang, H. Chang, Experimental study of hollow fiber AGMD modules with energy recovery foe water desalination, Desalination, 344 (2014) 55–63.
[2] A. Alkhudhiri, N. Darwish, N. Hilal, Membrane distillation: a comprehensive review, Desalination, 287 (2012) 2–18.
[3] B.V. Bruggen, C. Vandecasteele, Exergy and thermo-economic analysis of solar thermal cycles powered multi-stage flash desalination process, Desalination, 143 (2002) 207–218.
[4] E. Drioli, A. Criscuoli, E. Curcio, Membrane Contactors: Fundamentals, Applications and Potentialities, Membrane Science and Technology Series 11, Elsevier, 516 Amsterdam, Netherlands, 2006.
[5] M.S. El-Bourawi, Z. Ding, R. Ma, M. Khayet, A framework for better understanding membrane distillation separation process, J. Membr. Sci., 285 (2006) 4–29.
[6] M. Qtaishat, M. Khayet, T. Matsuura, Guidelines for preparation of higher flux hydrophobic/hydrophilic composite membranes for membrane distillation, J. Membr. Sci., 329 (2009) 193–200.
[7] A. Boubakri, A. Hafiane, S.A.T. Bouguecha, Direct contact membrane distillation: capability to desalt raw water, Arabian J. Chem., 10 (2014) S3475–S3481.
[8] S. Adham, A. Hussain, J.M. Matar, Application of membrane distillation for desalting brines from thermal desalination plants, Desalination, 314 (2013) 101–108.
[9] M.R. Qtaishat, F. Banat, Desalination by solar powered membrane distillation systems, Desalination, 308 (2013) 186–197.
[10] J.P. Mericq, S. Laborie, C. Cabassud, Vacuum membrane distillation of seawater reverse osmosis brines, Water Res., 44 (2010) 5260–5273.
[11] L.M. Camacho, L. Dumée, J. Zhang, J. Li, M. Duke, J. Gomez, S. Gray, Advances in membrane distillation for water desalination and purification applications, Water, 5 (2013) 94–196.
[12] R. Thiruvenkatachari, M. Manickam, T.O. Kwon, S. Moon, J.W. Kim, Separation of water and nitric acid with porous hydrophobic membrane by air gap membrane distillation (AGMD), Sep. Sci. Technol., 41 (2013) 3187–3199.
[13] A.M. Alklaibi, N. Lior, Transport analysis of air-gap membrane distillation, J. Membr. Sci., 255 (2005) 239–253.
[14] J. Kim, S.E. Park, T.S. Kim, D.Y. Jeong, K.H. Ko, Isotopic water separation using AGMD and VEMD, Nukleonika, 4 (2004) 137–142.
[15] H. Geng, H. Wu, P. Li, Q. He, Study on a new air-gap membrane distillation module for desalination, Desalination, 334 (2014) 29–38.
[16] J. Xu, Y.B. Singh, G.L. Amy, N. Ghaffour, Effect of operating parameters and membrane characteristics on air gap membrane distillation performance for the treatment of highly saline water, J. Membr. Sci., 512 (2016) 73–82.
[17] U. Dehesa-Carrasco, C.A. Pérez-Rábago, C.A. Arancibia-Bulnes, Experimental evaluation and modeling of internal temperatures in an air gap membrane distillation unit, Desalination, 326 (2013) 47–54.

[18] A. Alkhudhiri, N. Darwish, N. Hilal, Treatment of saline solutions using air gap membrane distillation: experimental study, Desalination, 323 (2013) 2–7.
[19] M. Asghari, A. Harandizadeh, M. Dhghani, Persian Gulf desalination using air gap membrane distillation: numerical simulation and theoretical study, Desalination, 374 (2015) 92–100.
[20] A. Boubakri, A. Hafiane, S.A.T. Bouguecha, Nitrate removal from aqueous solution by direct contact membrane distillation using two different commercial membranes, Desal. Wat. Treat., 56 (2015) 2723–2730.
[21] A. Boubakri, A. Hafiane, S.A.T. Bouguecha, Application of response surface methodology for modeling and optimization of membrane distillation desalination process, Ind. Eng. Chem. Res., 20 (2014) 3163–3169.
[22] P. Pal, A.K. Manna, Removal of arsenic from contaminated groundwater by solar-driven membrane distillation using three different commercial membranes, Water Res., 44 (2010) 5750–5760.
[23] M. Qtaishat, T. Matsuura, B. Kruczek, M. Khayet, Heat and mass transfer analysis in direct contact membrane distillation, Desalination, 219 (2008) 272–292.
[24] C.J. Geankoplis, Transport Processes and Unit Operations, 3rd Ed., Prentice-Hall International, USA, 1993.
[25] C.M. Guiji, G. Racz, J.W. Heuven, T. Reith, A.B. Haan, Modelling of a transmembrane evaporation module for desalination of seawater, Desalination, 126 (1999) 119–125.
[26] J. Phattaranawik, R. Jiraratananon, A.G. Fane, Effect of pore size distribution and air flux on mass transport in direct contact membrane distillation, J. Membr. Sci., 215 (2003) 75–85.
[27] A. Boubakri, S.A.T. Bouguecha, I. Dhaouadi, A. Hafiane, Effect of operating parameters on boron removal from seawater using membrane distillation process, Desalination, 373 (2015) 86–93.
[28] M.C. Garcia-Payo, M.A. Izquierdo-Gil, C. Fernàndez-Pineda, Air gap membrane distillation of aqueous alcohol solutions, J. Membr. Sci., 169 (2000) 61–80.
[29] R. Bahar, Conversion of Saline Water to Fresh Water Using Air Gap Membrane Distillation (AGMD), Thesis, 2010.
[30] S. Bouguecha, R. Chouikh, M. Dhahbi, Numerical study of the coupled heat and mass transfer in membrane distillation, Desalination, 152 (2002) 245–252.
[31] M. Khayet, Membranes and theoretical modeling of membrane distillation: a review, Adv. Colloid Interface Sci., 164 (2011) 56–88.
[32] L.H. Cheng, P.C. Wu, J. Chen, Numerical simulation and optimal design of AGMD-based hollow fiber modules for desalination, Ind. Eng. Chem. Res., 48 (2009) 4948–4959.